Optical spin- and current-injection study on Si(111)-In surfaces

N. Arzate,* R. A. Vázquez-Nava, and Bernardo S. Mendoza
Centro de Investigaciones en Óptica, León, Guanajuato, Mexico
(Received 9 September 2014; revised manuscript received 14 November 2014; published 24 November 2014)

We present a theoretical study of the optical generation of one-photon spin and current injection onto In-adsorbed Si(111) surfaces with 4×2 and 8×2 reconstructions. The spin injection, under incidence of circularly polarized light into nonmagnetic semiconductors, creates spin-polarized electrons in the conduction bands. The current injection is a nonlinear second-order effect that is allowed in materials without inversion symmetry. In bulk centrosymmetric crystals, the optical injection of current can only be observed at the surface wherein the inversion of symmetry might be broken. We report calculations for the degree of spin polarization and current-injection spectra which are calculated in a full electronic band structure scheme at the level of GW scissor-energy correction. Our results show an anisotropic behavior of the spin- and current-injection optical response. We obtain maximum percentages of the degree of spin polarization of 30% and 35% for the 4×2 and 8×2 surface reconstructions, respectively. It is also possible to optically generate injection current coming mainly from the first two top layers on both In-adsorbed surface reconstructions.

DOI: 10.1103/PhysRevB.90.205310 PACS number(s): 78.68.+m, 71.15.Mb, 73.20.At, 72.25.Fe

I. INTRODUCTION

An active research area is the study of one-dimensional (1D) arrays of atoms on surfaces. These kind of structures present interesting physical properties and have potential applications in nanoelectronics. Spin-charge separation as well as the formation of charge- or spin-density waves due to Peierls instability are examples of phenomena that can take place on such structures [1,2]. The 1D self-assembled array of indium (In) atoms adsorbed on the Si(111) surface is one of the systems that has been studied by the scientific community [3–10]. This surface presents three different phases: the 4×1, 4×2, and 8×2 surface reconstructions. Figure 1 shows top views of their respective atomic models. The 4×1 surface reconstruction is a stable phase at room temperature and is characterized by two parallel zigzag chains of In atoms alternating with a zigzag chain of silicon atoms on top of an essentially unreconstructed substrate [3]. Meanwhile, on the surface 4×2 and 8×2 reconstructions, In atoms are bound by forming one-dimensional chains of hexagons, as shown in Figs. 1(b) and 1(c).

Recent studies of the In-adsorbed Si(111) surfaces focused on the mechanism and origin of their phase transitions [4–7]. For instance, González *et al.* [4,5] performed molecular dynamic calculations and showed that the 8×2 surface reconstruction has the lower energy and is stable at low temperature (LT). They explained that the ground state consists of insulating 4×2 In chains with a weak interchain coupling that induces opposite shear distortions in alternate chains, resulting in the formation of In hexagons. They related the metallicity of the In-adsorbed Si(111)-4×1 surface to the low energy cost for shear distortion. More recently, González *et al.* [6] made a comparison between experimental scanning tunneling microscopy (STM) images of the LT 8×2 phase with STM image calculations from density functional theory (DFT). Their LT studies indicated the existence of a frozen shear distortion between neighboring atomic chains. Furthermore, they showed tunneling spectra indicating that the metal-insulator (MI) transition coincides with the collapse of the surface-state energy band gap at the Γ point of the 4×2 Brillouin zone (BZ) which implied that the MI transition is driven by a shear phonon. Later, Wippermann *et al.* [7] performed free-energy calculations based on DFT and concluded that the MI phase transition is caused by the gain in mainly vibrational entropy that overcompensates, for higher temperatures, the gain in band structure energy realized upon transforming the metallic In zigzag chains into semiconducting In hexagons. Soft shear and rotary vibrations drive the transformation between the In zigzag chains stable at room temperature and the hexagons formed at low temperatures.

Chandola *et al.* studied the In-adsorbed surface through experimental midinfrared optical measurements and *ab initio* calculations of the anisotropic optical response of the surface [8]. Through infrared spectroscopy ellipsometry and reflectance anisotropy spectroscopy of the 8×2 phase, they showed that the anisotropic Drude tail of the metallic phase is replaced by two peaks at 0.50 and 0.72 eV, which appear in *ab initio* optical response calculations for the hexagon model of the 8×2 structure. More recent reports performed measurements of the anisotropic behavior of the conductivity of the In-adsorbed Si(111) surface [9,10], wherein the parallel conductivity to the In chains was found to be larger than the perpendicular conductivity.

In this paper, we are interested in phenomena that have been recently studied on semiconducting surfaces: the one-photon optical spin and current injection. There are theoretical reports of calculations for the spin injection in bulk media, for instance, GaAs, Si, CdSe, and Ge semiconductors [11–13]. A report of spin injection at surfaces was performed by Mendoza and Cabellos [14]. They studied the As- and In-covered Si(111) as well as the Sb-covered GaAs(110) surfaces. We follow their analysis to calculate the spin- and current-injection response. Here we are interested in studying these phenomena on the In-adsorbed Si(111) surfaces with 4×2 and 8×2 reconstructions which present a semiconducting character. The optical spin injection for surfaces might be characterized through the physical dimensionless quantity of degree of spin

*narzate@cio.mx

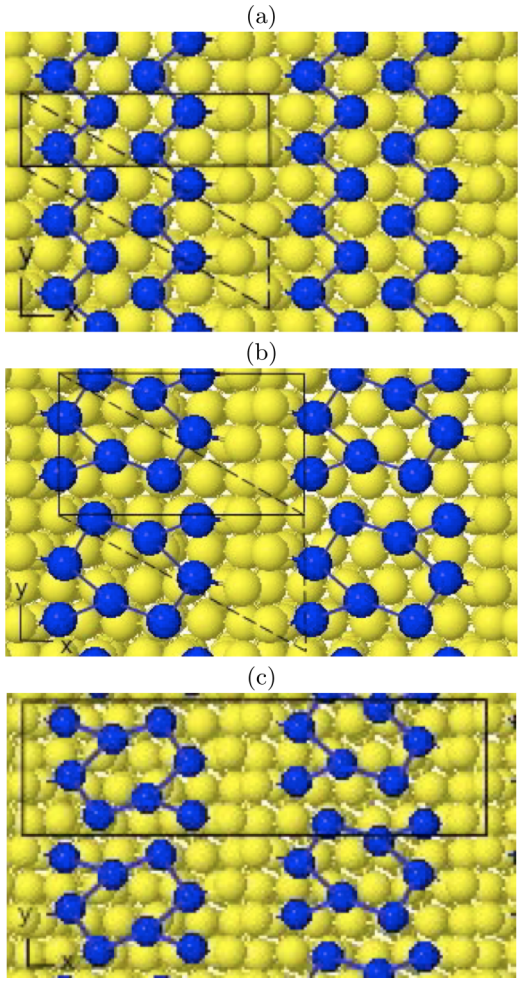

FIG. 1. (Color online) Top views of the In-adsorbed Si(111) surface reconstructions: (a) 4×1, (b) 4×2, and (c) 8×2. The dark (blue) and light (yellow) circles represent the In and Si atoms, respectively. The x and y directions are along the $[11\bar{2}]$ and [110] crystallographic directions, correspondingly. The possible rectangular and diagonal unit cells are defined by continuous and dotted lines.

polarization (DSP), $\mathcal{D}^{s}(\omega)$, which is a function of the photon frequency, ω. Meanwhile the one-photon current injection is characterized by the current injection tensor, $\boldsymbol{\eta}^{s}(0;\omega,-\omega)$, which is a particular case of the current injection tensor $\boldsymbol{\eta}^{s}(\omega_1-\omega_2;\omega_1,-\omega_2)$, where ω_1 and ω_2 are the frequencies of two different optical fields. We write the frequency dependence of the injection current tensor as $\boldsymbol{\eta}^{s}(\omega)$ instead of $\boldsymbol{\eta}^{s}(0;\omega,-\omega)$. Note that these calculations are on one-dimensional atomic arrays adsorbed on surfaces.

The organization of the paper is as follows. First, in Sec. II, we explain phenomenologically the effects of optical spin and current injection and give a brief account of their theory. The descriptions of both phenomena are given in the independent-particle approximation. Second, in Sec. III, we describe details of the calculation of the optical response and show our calculations for the corresponding spectra of $\mathcal{D}_i^{s}(\omega)$ and $\boldsymbol{\eta}^{s}(\omega)$ for the respective studied In-adsorbed Si(111) surfaces. Finally, we give conclusions in Sec. IV.

II. THEORY

A. Optical spin injection

The injection of spin-polarized electrons into nonmagnetic materials is a very interesting phenomenon which has a great potential for applications in the field of spintronics [15–19]. Optical spin injection of carriers takes place when circularly polarized light [20] falls on a semiconducting material and injects spin-polarized electrons from the valence into the conduction bands. It occurs as a result of the interaction of electron spin and motion caused by the spin-orbit coupling in the material. The DSP quantifies the fraction of injected electrons into the conduction bands that are spin polarized. It can be calculated by full band structure local-density approximation (LDA) and $\mathbf{k}\cdot\mathbf{p}$ methods [11,12].

Surfaces covered with adsorbates are potential systems for spin injection [14]. Mendoza and Cabellos derived expressions for the optical spin generation suitable for surfaces and interfaces [14]. They used a slab approach in order to model the surface. In their layer-by-layer formalism, they separated the response of any layer of the slab through the use of a cut function that selects the contribution to the optical response of a given layer. They wrote the surface DSP along direction i as

$$\mathcal{D}_i^{s}(\omega)=\frac{-2i\zeta_{ixy}^{s}(\omega)}{\hbar(\xi_{xx}^{s}(\omega)+\xi_{yy}^{s}(\omega))/2}, \tag{1}$$

where $\zeta_{ijk}^{s}(\omega)$ are the surface spin-injection rate tensor components, and $\xi_{jj}^{s}(\omega)$ are diagonal components of the surface carrier generation rate tensor. Here i,j,k denote Cartesian directions. The superscript "s" in the physical quantities of Eq. (1) indicates that the response corresponds to that of the surface or the semi-infinite crystal, which includes the top surface layer and all half-slab subsurface layers. In our calculation, we consider the normal incidence of circularly polarized light propagating along the $-z$ direction, $\mathbf{E}(\omega)=E_0(\hat{x}-i\hat{y})/\sqrt{2}$, where E_0 is the field intensity. Since $\mathbf{E}(\omega)$ lies on the plane of the surface, it can be taken, with the usual neglect of local field corrections, as uniform through the interface region. See Ref. [14] for a full account. Taking into account the fact that it is possible to inject spin-polarized electrons to the conduction bands along the three orthogonal directions with incidence of light on the surface plane, the total DSP can be obtained by the relation $|\mathcal{D}^{s}(\omega)|=\{[\mathcal{D}_x^{s}(\omega)]^2+[\mathcal{D}_y^{s}(\omega)]^2+[\mathcal{D}_z^{s}(\omega)]^2\}^{1/2}$.

B. Optical current injection

The optical injection of current is a second-order optical nonlinear effect and has been the subject of research in recent years [21–26]. In noncentrosymmetric crystals, an observable photocurrent can be injected with a single optical beam [26–28]. The injection current in crystals arises from the interference of one-photon absorption processes associated with different linear polarizations of the light [28]. When the crystal is photoexcited with circularly polarized light, the different excitation pathways for the two orthogonal polarization components lead to an interference effect, resulting in an asymmetric population of the injected carriers in reciprocal space and, hence, a current. Since it is generated with circularly polarized light, the generation of injection

current is also called the *circular photovoltaic effect* [29]. It has been proposed that photocurrents can be generated not only in bulk semiconductors but also in one-dimensional (1D) nanotubes [30,31] and two-dimensional (2D) systems such as in the GaAs(110) surface [32]. Mele and Král have shown that two-color (or two-beam) photocurrents can be injected in unbiased carbon nanotubes [30]. This, however, is a third-order nonlinear optical effect analogous to the effect proposed by Atanasov *et al.* [25] Although the two-color injection current has been observed in GaAs [24], the experimental setup is more complicated than that of the one-beam injection current.

The current injection is allowed in materials without center-of-inversion symmetry. There are 21 of the 32 crystal classes that lack inversion symmetry, but the injection current is only nonzero for 18. Crystals with classes $\bar{6}m2$, $\bar{6}$, and $\bar{4}\bar{3}m$ are the exceptions. For instance, the injection current is forbidden in zinc-blende GaAs whose crystal class is the last of those mentioned above. Bulk centrosymmetric crystals might lose their inversion symmetry at their surface. Hence, at surfaces such as the In-adsorbed Si(111) surface, the generation of photocurrents would be possible. In the process of current injection, the energy increase of the injected carriers is provided by the electromagnetic field; meanwhile, the increase in momentum is provided by the crystal lattice.

Cabellos *et al.* [33] derived expressions for the generation rate of the injection current suitable for surfaces and interfaces. Applying the same layer-by-layer formalism as that used for the calculation for $\mathcal{D}_i^{\rm s}(\omega)$, they defined the surface injection current as

$$\dot{\mathbf{J}}_i^{\rm s,inj}(\omega) = \eta_{ijk}^{\rm s}(\omega) E_j(\omega) E_k(-\omega), \tag{2}$$

where $\eta_{ijk}^{\rm s}(\omega)$ is the surface injection current tensor which quantifies the injection current along direction i that is optically injected by two electric fields polarized along directions j and k, respectively. For a surface system with centrosymmetric bulk, it is given by

$$\eta_{ijk}^{\rm s}(\omega) = l_{\rm eff} \sum_{l=1}^{N_{\rm eff}} \eta_{ijk}(l|\omega), \tag{3}$$

where $\eta_{ijk}(l|\omega)$ gives the corresponding lth layer contribution to the surface injection current tensor. The sum in Eq. (3) is carried out from the top layer, $l = 1$, to $l = N_{\rm eff}$. That is, the surface injection current tensor spectrum mainly has contributions of the first $N_{\rm eff}$ surface layers that extend to an effective length, $l_{\rm eff}$. The tensor $\eta_{ijk}^{\rm s}(\omega)$ is purely imaginary and has the property of being antisymmetric in the last two Cartesian indices, j and k [28,34]. Since incidence of light circularly polarized on the surface plane might generate injection current along the three orthogonal directions, we take $|\eta^{\rm s}(\omega)| = \{[\eta_{xyx}^{\rm s}(\omega)]^2 + [\eta_{yyx}^{\rm s}(\omega)]^2 + [\eta_{zyx}^{\rm s}(\omega)]^2\}^{1/2}$ as the total injection current value. For surfaces, $\eta_{zyx}^{\rm s}(\omega)$ is negligible. The units of both $\dot{\mathbf{J}}^{\rm s,inj}(\omega)$ and $\eta_{ijk}^{\rm s}(\omega)$ are those of their bulk counterparts times that of length. See Ref. [33] for full details. In the following, we omit the frequency dependence of $\mathcal{D}_i^{\rm s}(\omega)$ and $\eta_{ijk}^{\rm s}(\omega)$ for ease of handling.

III. RESULTS

We have performed numerical calculations for $\mathcal{D}_i^{\rm s}$ and $\eta_{iyx}^{\rm s}$ for the 4×2 and 8×2 In-adsorbed Si(111) surfaces. The theoretically determined 4×2 reconstruction of the Si(111)-In surface was used as a reference [5]. Hence we have considered a centrosymmetric slab comprised of 12 bulk atomic Si layers plus the front and back surface layers, which comprise two surface layers: the top In-adsorbed atomic layer and a layer with four Si atoms per 4×2 surface unit cell. A vacuum length of at least eight atomic layers was taken. The self-consistent ground state and their Kohn-Sham states were calculated in the framework of DFT within the LDA, with the use of the plane-wave ABINIT code [35]. We have used the relativistic separable dual-space Gaussian pseudopotentials of Hartwigsen-Goedecker-Hutter [36]. We have included the spin-orbit interaction, which is required, in the calculations for $\boldsymbol{\mathcal{D}}^{\rm s}$ but not in those for $\boldsymbol{\eta}^{\rm s}$, where it could be omitted. The contribution of semicore states in an optics calculation for Si is negligible. Meanwhile, it might be important for heavy atoms such as In. However, their inclusion in the calculations has the cost of significantly increasing the computational resources. In order to keep the calculation feasible, in our calculations we have not taken semicore states into consideration. Furthermore, we have taken a cutoff energy of 10 and 5 Ha for the 4×2 and 8×2 surface reconstructions, respectively.

The correction to the LDA energy band gap was done through a many-body G_0W_0 calculation just at the $\mathbf{\Gamma}$ point, and at the level of a scissors rigid shift to the conduction bands [37,38]. In the calculation of the quasiparticle energies, we have employed the plasmon pole approximation for the screening potential. In order to avoid the Coulomb interaction between contiguous cells, a Coulomb cutoff length in the direction perpendicular to the surface of 15 Bohrs was considered. The energy eigenvalues and matrix elements were calculated by using 36 $\mathbf{k}$ points in the irreducible BZ.

Figures 2 and 3 show band structures calculated within DFT-LDA of the In-adsorbed Si(111) surface reconstructions

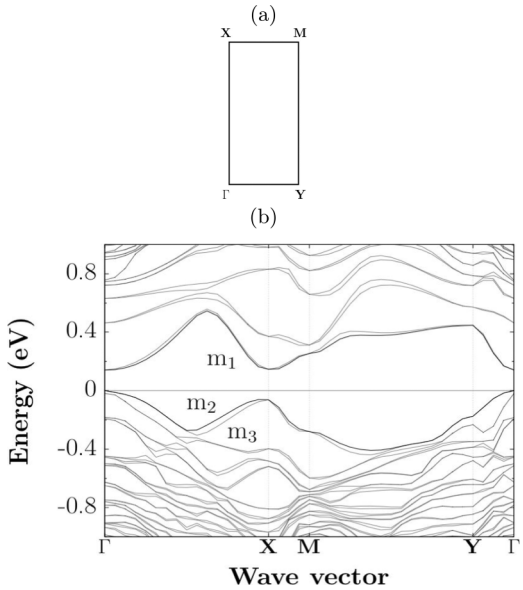

FIG. 2. (a) Brillouin zone and (b) LDA band structure of the Si(111)-In 4×2 surface. Spin-orbit interaction was considered in the calculation.

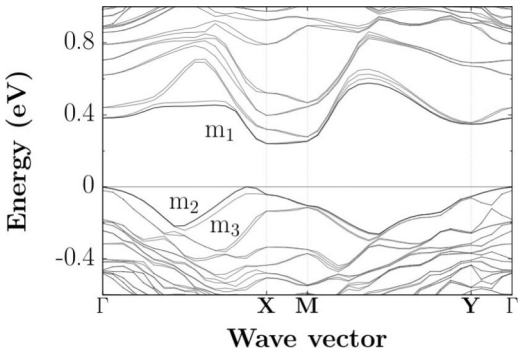

FIG. 3. LDA band structure of the Si(111)-In 8 × 2 surface. Spin-orbit interaction was considered in the calculation.

4 × 2 and 8 × 2, respectively. The path **Γ**-**X** is along the In atomic chains. Overall, the calculated band structures of Figs. 2 and 3 are qualitatively in good agreement with those calculated by González *et al.* [5] and Chandola *et al.* [8]. Both band structures have an insulating character and are characterized by an LDA energy band gap of the spin-split surface states, m_1 and m_2. The maximum valence bands of both the 4 × 2 and 8 × 2 surface reconstructions show maximum spin splittings of about 40 meV along the **Γ**-**X** path. The 4 × 2 surface reconstruction has a direct energy band gap of 0.14 eV at **Γ**; whereas the 8 × 2 surface reconstruction has an indirect energy band gap of 0.24 eV at around **X**. Those theoretical values are within the range of 0.1–0.3 (±0.05) eV of the experimental energy band-gap measurements for the low-temperature phases [39–44]. We note that our calculated band structure for the 8 × 2 shows a small indirect energy band gap, in contrast to that calculated by Chandola *et al.* [8] wherein this indirect band gap is almost zero. The GW band-gap energy corrections that we have obtained are 0.25 and 0.43 eV for the 4 × 2 and 8 × 2 surface reconstructions, respectively. These values are comparable to those scissors shifts already reported or applied. For instance, Stekolnikov *et al.* performed GW calculations for high-symmetry **k** points of the 4 × 2 surface BZ and found that self-energy effects increase the transition energies by 0.26 eV on average [45]. Furthermore, a rigid scissors shift of 0.50 eV has been applied in calculated optical spectra [8,46] to account for optical transitions that involve bulk silicon states [47].

Figures 4(a) and 4(b) show spectra for $\mathcal{D}_i^s$ of the In-adsorbed Si(111) surface with reconstructions 4 × 2 and 8 × 2, respectively. The plus (minus) sign of $\mathcal{D}_i^s$ defines the positive (negative) direction of the spin polarization along i. It can be observed that $\mathcal{D}_i^s$ have an onset, wherein the system starts absorbing, just at the band-gap energy of the corresponding surface. In both the 4 × 2 and the 8 × 2 surfaces, the respective spectrum for the $\mathcal{D}_z^s$ component has the highest absolute value for the DSP. On the one hand, the two small structures just above the band-gap energy shown in the $\mathcal{D}_z^s$ spectrum [see Fig. 2(a)], for the 4 × 2 surface reconstruction, come from contributions of **k** points at around **Γ** and along the path **Γ**-**X**, respectively, that relate transitions between the spin-split surface states m_2 and m_1. The negative peak at 0.64 mainly has its origin in transitions between the spin-split surface states m_2 and m_1 that take place along the path **Γ**-**X**-**M**. On the other hand, the related transitions that are involved

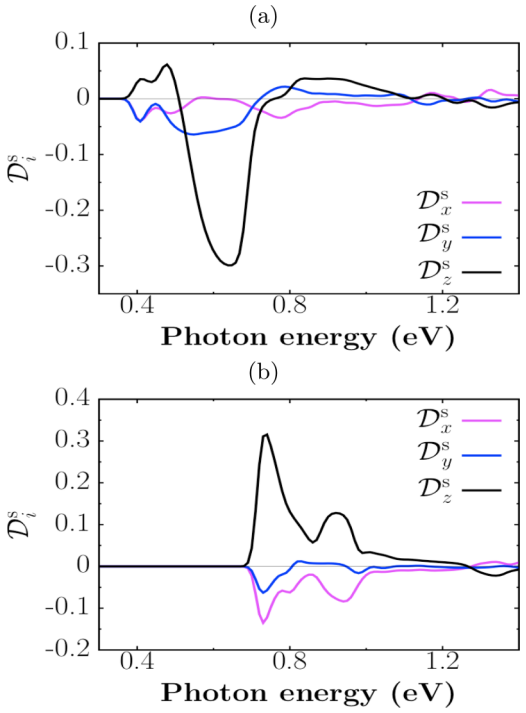

FIG. 4. (Color online) Spectra of the surface degree of spin polarization along direction i, $\mathcal{D}_i^s$, for the reconstructions (a) 4 × 2 and (b) 8 × 2 of the Si(111)-In surface under incidence of circularly polarized light.

in the maxima of the $\mathcal{D}_z^s$ spectrum for the 8 × 2 surface reconstruction are as follows: the peak at 0.74 has contributions of transitions between the spin-split maximum valence and minimum conduction bands at around the **X** point; meanwhile, the second maximum at 0.92 eV mainly has contributions of different **k** points close to the path **Γ**-**X**, relating transitions between either of the last four valence bands and either of the first six conduction bands. Hence the origin of the main features of the $\mathcal{D}_z^s$ spectra is surface related and can be ascribed to the behavior of the band structure of the particular In-adsorbed surface reconstruction.

Table I shows a comparison of the reported values for the highest percentage of $|\mathcal{D}_z|$ for other surfaces and bulk systems. As we can see from the table, the studied Si(111)-In 4 × 2 and the 8 × 2 surfaces have the lower absolute values for $\mathcal{D}_z^s$ compared to those corresponding to other Si(111) and GaAs(110) surfaces, and bulk systems. However, they present similar maximum absolute values $\mathcal{D}_z^s \sim 30\%$ as that of bulk Si with a difference in the lower photon energy wherein their maxima are reached. This makes the use of light sources in another range of energy possible. It is worthwhile to note that the optical spin-injection response of the In-adsorbed Si(111) surfaces is anisotropic. This fact makes the spin injection a selective tool for surface characterization. Hence, for the Si(111)-In 4 × 2 surface, $|\mathcal{D}^s| = 30\%$ at the photon energy of 0.64 eV; meanwhile, for the Si(111)-In 8 × 2 surface, the maximum percentage of $|\mathcal{D}^s|$ is 35% at the photon energy of 0.74 eV, just 0.07 eV above the quasiparticle band-gap energy.

We show, in Figs. 5 and 6, spectra of the injection current tensor components η_{xyx} and η_{yyx}, corresponding to

TABLE I. Comparison of the reported values for the highest percentage of degree of spin polarization along direction z for some surfaces and bulk systems.

Structure	Energy (eV)	$\lvert\mathcal{D}_z\rvert$ (%)	Reference
Si(111)-In 8×2	0.74	32	This work
Si(111)-In 4×2	0.64	30	This work
Si(111)-In $\sqrt{3} \times \sqrt{3}$ R30°	2.00	44	[14]
Si(111)-As 1×1	2.20	100	[14]
GaAs(110)-clean 1×1	1.64	90	[14]
GaAs(110)-Sb 1×1	0.84	52	[14]
Bulk Si	3.44	30	[11]
Bulk Ge	0.90	50	[13]
Bulk GaAs	1.50	50	[11,22]
Bulk CdSe	1.80	100	[11]

the contributions of the first four layers for the In-adsorbed Si(111) 4×2 and 8×2 surfaces, respectively. The respective spectra of the surface or total injection current tensor η^{s}_{iyx} are also plotted. We observe from these figures that light circularly polarized on the plane x-y that fall on the In-adsorbed Si(111) surface would generate injection current along both directions x (perpendicular) and y (parallel) to the In chains. Injection current along z or perpendicular direction to the surface vanishes. The plus (minus) sign of both η_{iyx} and η^{s}_{iyx} indicates the positive (negative) direction of the injection current along i.

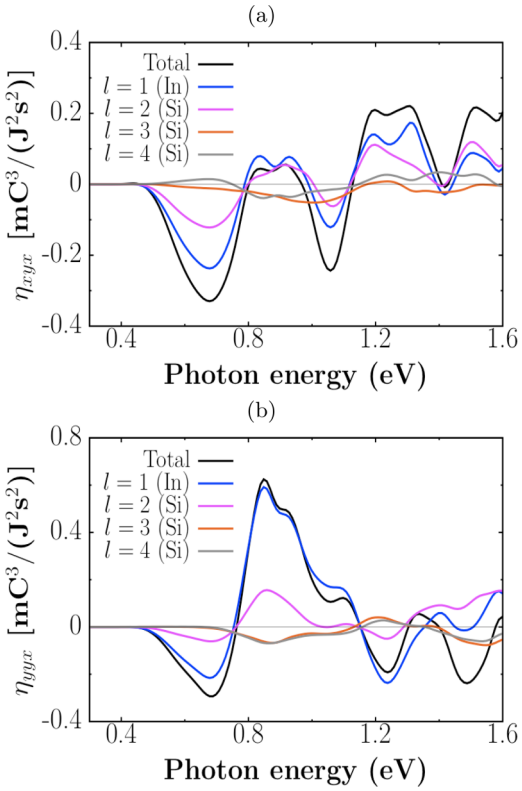

FIG. 5. (Color online) Spectra of the injection current tensor components, (a) η_{xyx} and (b) η_{yyx}, for the 4×2 reconstruction of the Si(111)-In surface. The plot shows different surface layer contributions to the respective surface or total spectra, η^{s}_{iyx}.

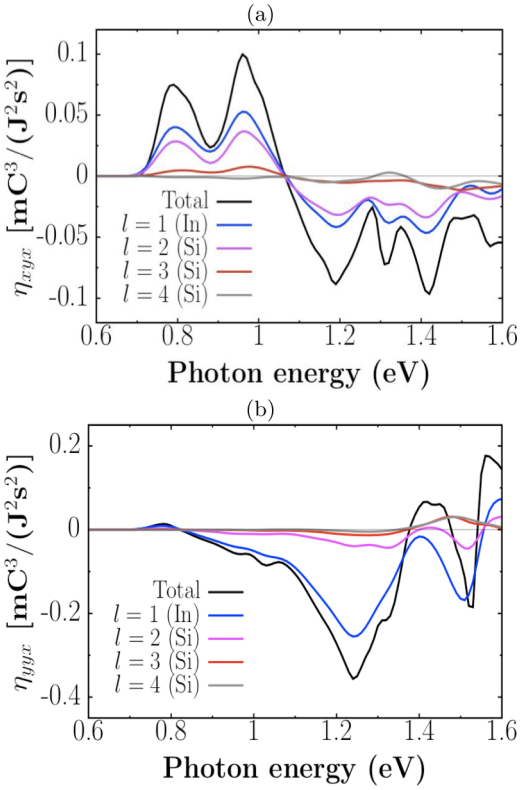

FIG. 6. (Color online) Spectra of the injection current tensor components, (a) η_{xyx} and (b) η_{yyx}, for the 8×2 reconstruction of the Si(111)-In surface. The plot shows different surface layer contributions to the respective surface or total spectra, η^{s}_{iyx}.

The spectra of the injection current tensor have their onset just at the respective band-gap energy value and show various local minima or maxima in the plotted photon energy range. We can also observe from Fig. 5 that overall the main contributions to the different features shown in the injection current tensor come from the first two atomic layers, i.e., the In atomic layer and the first Si layer, which contains four Si atoms per 4×2 unit cell. Contributions to the total injection current spectra that originate from layers $l > 4$ are negligible. Thus we have considered in the calculation for η^{s}_{ijk} that the effective length [see Eq. (3)] comprises the first four layers, given the value of $l_{\text{eff}} = 7.2$ Å.

An analysis of the different layer contributions to the total injection current tensor spectra gives information about the direction and particular atomic layers where the injection current might be generated. We perform such an analysis from Figs. 5 and 6. For both studied surface reconstructions, the injection current is generated parallel to the surface plane; its respective component that is perpendicular to the surface plane vanishes. First, we focus on some of the features seen in the spectra corresponding to the 4×2 surface reconstruction. The peaks seen at 0.68 eV of the spectra for η^{s}_{xxy} and η^{s}_{yxy} are both negative and are almost equal in magnitude. Thus injection current is generated along both directions parallel and perpendicular to the In atomic chains. These features have main contributions from the first two atomic layers. The positive peak observed at 0.85 eV of the η^{s}_{yxy} spectrum has a relative magnitude that is 17 times bigger than that of η^{s}_{xxy} at

this same photon energy. Hence the injection current generated is mainly directed parallel to the In atomic chains. Besides, we can observe from Fig. 5(b) that this feature observed at 0.85 eV of the η^{s}_{yxy} spectrum is almost totally generated along the first atomic layer. The contribution of the second layer has a positive contribution, whereas the contributions of the third and fourth layers have negative values and both contributions sum up negatively. Although we can see that there are also contributions from the second to the fourth atomic layers, their contributions cancel each other, leaving almost the effective contribution of the first layer.

Meanwhile, some of the features observed in the spectra corresponding to the 8×2 surface reconstruction are as follows: the lower positive peak at 0.79 eV of η^{s}_{xxy} has a magnitude almost ten times bigger than the respective magnitude of η^{s}_{yxy}. Thus the injection current generated at 0.79 eV is mainly directed perpendicular to the In atomic chains and mainly has contributions from the first two layers. The feature found at 0.96 eV in η^{s}_{xxy} has a comparable magnitude to that of η^{s}_{yxy}. Thus, at the photon energy of 0.96 eV, the injection current is generated in both directions parallel and perpendicular to the In atomic chains. The injection current directed perpendicular (parallel) to the In chains mainly has contributions from the first two layers (first layer). Finally, the negative peak at 1.24 eV of η^{s}_{yxy} has a relative magnitude that is six times bigger than that of η^{s}_{xxy} and it has a main contribution from the In atomic chain. Thus, at the photon energy of 1.24 eV, the injection current is mainly generated along the In atomic chains.

The large dispersion of the band structure of the 4×2 and 8×2 reconstructions of the In-adsorbed Si(111) surface allows their optical response to have contributions that come from transitions taking place at different points in the BZ. We address each of the main peak structures for η^{s}_{iyx} considering a band structure with no spin-orbit interaction, as mentioned before. On the one hand, with respect to the 4×2 surface reconstruction, the minima at 0.68 and 1.06 eV of the η^{s}_{xyx} spectrum shown in Fig. 5 have major contributions that originate in transitions between surface states, the maximum valence, and the minimum conduction bands. Meanwhile, the maximum peak at 0.85 eV shown in η^{s}_{yyx} mainly has contributions from transitions that take place between the maximum valence band and either of the first two conduction bands. On the other hand, the main structures of the optical response of the 8×2 surface reconstruction shown in Fig. 6 have the following main contributions: for η^{s}_{xyx}, the peak at 0.79 eV originates from transitions between the maximum valence and the minimum conduction band; and the peak at 0.96 eV has major contributions from transitions between the maximum valence band and any one of the first three conduction bands. Hence, these structures shown in the spectra of injection current tensor for photon energies of less than 1.1 eV are surface related, whereas the minimum at 1.24 eV of η^{s}_{yyx} has its origin in transitions that take place between any one of the last eight valence bands and either of the first two conduction bands. Thus, in the process of current injection in the studied In-adsorbed surfaces, the charge is mainly allowed to move on or among the top first four layers and the electronic transitions that contribute to the injection current response take place between surface and surface or bulk and surface electronic states. The surface reconstruction determines the semiconducting behavior of the band structure, which in turn rules the anisotropic behavior of the optical injection current response.

TABLE II. Comparison of the highest reported absolute value of the surface injection current tensor component η^{s}_{yyx} for some surface and bulk systems.

Structure	Energy (eV)	$\lvert\eta^{s}_{yyx}\rvert$ ($mC^3/J^2\ s^2$)	Reference
Si(111)-In 8×2	1.24	0.35	This work
Si(111)-In 4×2	0.85	0.63	This work
Si(111) 2×1	0.75	1.22	[33]
GaAs(110) clean	4.30	0.30	[33]
Gas(110)-Sb	4.60	0.17	[33]
Bulk CdSe	1.80	$\lvert\eta^{s}_{yyz}\rvert = 90$	[26]

Table II tabulates the highest values of the surface injection current tensor component η^{s}_{yyx} that have been calculated on some surface systems. We observe that the Si(111) 2×1 and the Si(111)-In 4×2 are the surfaces wherein the injection current tensor has higher values within the same order of magnitude. Meanwhile, the Si(111) 8×2 surface presents an injection current tensor value similar to that of the clean GaAs(110) surface, but for a lower photon energy. The calculated total absolute values $|\eta^{s}|$ are 0.36 and 0.63 $mC^3/J^2\ s^2$ at the photon energies of 1.24 and 0.85 eV, respectively, for the respective 8×2 and 4×2 surface reconstructions. Laman *et al.* [26] performed one-photon experiments for the injection current on bulk CdSe and measured an injection current density of 2 $\mu A/cm^2$ that penetrated 1.8 μm. In Table II, we also show the corresponding experimental value for the surface injection current tensor of bulk CdSe. It is worthwhile to mention that the measurements of injection current done by Laman *et al.* were performed with low incident light intensity of 0.06 W/cm^2. Since the current signal scales linearly with the field intensity, an observable injection current signal from the surface must take place with field intensities low enough to avoid surface damage.

IV. CONCLUSIONS

We have performed *ab initio* calculations for the spin and injection current on In-adsorbed Si(111) 4×2 and 8×2 surfaces. The surface spin- and current-injection response is very sensitive to the symmetry characteristics of the surface and shows an anisotropic behavior. It is possible to inject spin-polarized electrons along the perpendicular direction to the surface plane, obtaining a surface degree of spin polarization of the injected electrons of about 30% and 35% at the photon energies of around 0.64 and 0.74 eV, for the 4×2 and 8×2 reconstructions of the In-adsorbed Si(111) surface, respectively. On the other hand, dealing with the injection of current with circularly polarized light with intensity of 0.1 W/cm^2, the estimation of the surface injection current density, on the 4×2 surface at the photon energy of 0.85 eV, is 0.76 nA/cm, whereas, for the 8×2 surface, the respective estimation is 0.42 nA/cm at the photon energy of 1.24 eV. According to measurements already done on bulk materials, it is actually possible to measure such amount of injection

current density. Thus the control of the motion of the electron at the In-adsorbed Si(111) surfaces is possible by incidence of circularly polarized light. In general, injection current is generated in both directions, parallel and perpendicular to the direction of the one-dimensional atomic chains, and mainly has contributions from the first two atomic layers corresponding to In and Si atomic chains. However, it is possible to select particular photon frequencies at which the injection current is mostly generated along the In atomic chains. Hence, the optical control and generation of both spin and current injection on one-dimensional arrays of adatoms on surfaces are possible phenomena that can be used either for surface characterization or practical applications.

ACKNOWLEDGMENT

This work has been partly supported by Consejo Nacional de Ciencia y Tecnología, Mexico, Grant No. 153930.

[1] H. W. Yeom, S. Takeda, E. Rotenberg, I. Matsuda, K. Horikoshi, J. Schaefer, C. M. Lee, S. D. Kevan, T. Ohta, T. Nagao, and S. Hasegawa, Phys. Rev. Lett. **82**, 4898 (1999).
[2] T. Aruga, J. Phys.: Condens. Matter **14**, 8393 (2002).
[3] O. Bunk, G. Falkenberg, J. H. Zeysing, L. Lottermoser, R. L. Johnson, M. Nielsen, F. Berg-Rasmussen, J. Baker, and R. Feidenhans'l, Phys. Rev. B **59**, 12228 (1999).
[4] C. González, J. Ortega, and F. Flores, New J. Phys. **7**, 100 (2005).
[5] C. González, F. Flores, and J. Ortega, Phys. Rev. Lett. **96**, 136101 (2006).
[6] C. González, J. Guo, J. Ortega, F. Flores, and H. H. Weitering, Phys. Rev. Lett. **102**, 115501 (2009).
[7] S. Wippermann and W. G. Schmidt, Phys. Rev. Lett. **105**, 126102 (2010).
[8] S. Chandola, K. Hinrichs, M. Gensch, N. Esser, S. Wippermann, W. G. Schmidt, F. Bechstedt, K. Fleischer, and J. F. McGilp, Phys. Rev. Lett. **102**, 226805 (2009).
[9] T. Uetake, T. Hirahara, Y. Ueda, N. Nagamura, R. Hobara, and S. Hasegawa, Phys. Rev. B **86**, 035325 (2012).
[10] W. G. Schmidt, S. Wippermann, S. Sanna, M. Babilon, N. J. Vollmers, and U. Gerstmann, Phys. Status Solidi B **249**, 343 (2012).
[11] F. Nastos, J. Rioux, M. Strimas-Mackey, B. S. Mendoza, and J. E. Sipe, Phys. Rev. B **76**, 205113 (2007).
[12] J. L. Cabellos, C. Salazar, and B. S. Mendoza, Phys. Rev. B **80**, 245204 (2009).
[13] J. Rioux and J. E. Sipe, Phys. Rev. B **81**, 155215 (2010).
[14] B. S. Mendoza and J. L. Cabellos, Phys. Rev. B **85**, 165324 (2012).
[15] I. Žutić, J. Fabian, and S. Das Sarma, Rev. Mod. Phys. **76**, 323 (2004).
[16] A. Fert, Rev. Mod. Phys. **80**, 1517 (2008).
[17] F. Pezzoli, F. Bottegoni, D. Trivedi, F. Ciccacci, A. Giorgioni, P. Li, S. Cecchi, E. Grilli, Y. Song, M. Guzzi, H. Dery, and G. Isella, Phys. Rev. Lett. **108**, 156603 (2012).
[18] F. Bottegoni, A. Ferrari, G. Isella, M. Finazzi, and F. Ciccacci, Phys. Rev. B **88**, 121201 (2013).
[19] F. Bottegoni, A. Ferrari, S. Cecchi, M. Finazzi, F. Ciccacci, and G. Isella, Appl. Phys. Lett. **102**, 152411 (2013).
[20] M. I. Dyakonov and V. I. Perel, in *Optical Orientation*, edited by F. Meier and B. P. Zakharchenya (Elsevier, New York, 1984), Chap. 2.
[21] F. Nastos and J. E. Sipe, Phys. Rev. B **74**, 035201 (2006).
[22] R. D. R. Bhat and J. E. Sipe, Phys. Rev. B **72**, 075205 (2005).
[23] J. M. Fraser, A. I. Shkrebtii, J. E. Sipe, and H. M. van Driel, Phys. Rev. Lett. **83**, 4192 (1999).
[24] A. Haché, Y. Kostoulas, R. Atanasov, J. L. P. Hughes, J. E. Sipe, and H. M. van Driel, Phys. Rev. Lett. **78**, 306 (1997).
[25] R. Atanasov, A. Haché, J. L. P. Hughes, H. M. van Driel, and J. E. Sipe, Phys. Rev. Lett. **76**, 1703 (1996).
[26] N. Laman, A. I. Shkrebtii, J. E. Sipe, and H. M. van Driel, Appl. Phys. Lett. **75**, 2581 (1999).
[27] D. Côte, N. Laman, and H. M. van Driel, Appl. Phys. Lett. **80**, 905 (2002).
[28] J. E. Sipe and A. I. Shkrebtii, Phys. Rev. B **61**, 5337 (2000).
[29] B. I. Sturman and V. M. Fridkin, *The Photovoltaic and Photorefractive Effects in Noncentrosymetric Materials* (Gordon and Breach Science, New York, 1992).
[30] E. J. Mele, P. Král, and D. Tománek, Phys. Rev. B **61**, 7669 (2000).
[31] P. Král, E. J. Mele, and D. Tománek, Phys. Rev. Lett. **85**, 1512 (2000).
[32] T. Rangel, M.S. thesis, Centro de Investigaciones en Óptica, 2006.
[33] J. L. Cabellos, B. S. Mendoza, and A. I. Shkrebtii, Phys. Rev. B **84**, 195326 (2011).
[34] F. Nastos and J. E. Sipe, Phys. Rev. B **82**, 235204 (2010).
[35] The ABINIT code is a common project of the Université Catholique de Louvain, Corning Incorporated, and other contributors (http://www.abinit.org); X. Gonze *et al.*, Comput. Mater. Sci. **25**, 478 (2002); Zeit. Crystallogr. **220**, 558 (2005).
[36] C. Hartwigsen, S. Goedecker, and J. Hutter, Phys. Rev. B **58**, 3641 (1998).
[37] R. Del Sole and R. Girlanda, Phys. Rev. B **48**, 11789 (1993).
[38] H. Hübener, E. Luppi, and V. Véniard, Phys. Rev. B **83**, 115205 (2011).
[39] O. Gallus, Th. Pillo, M. Hengsberger, P. Segovia, and Y. Baer, Eur. Phys. J. B **20**, 313 (2001).
[40] H. W. Yeom, K. Horikoshi, H. M. Zhang, K. Ono, and R. I. G. Uhrberg, Phys. Rev. B **65**, 241307 (2002).
[41] J. R. Ahn, J. H. Byun, H. Koh, E. Rotenberg, S. D. Kevan, and H. W. Yeom, Phys. Rev. Lett. **93**, 106401 (2004).
[42] S. J. Park, H. W. Yeom, S. H. Min, D. H. Park, and I.-W. Lyo, Phys. Rev. Lett. **93**, 106402 (2004).
[43] T. Tanikawa, I. Matsuda, T. Kanagawa, and S. Hasegawa, Phys. Rev. Lett. **93**, 016801 (2004).
[44] Y. J. Sun, S. Agario, S. Souma, K. Sugawara, Y. Tago, T. Sato, and T. Takahashi, Phys. Rev. B **77**, 125115 (2008).
[45] A. A. Stekolnikov, K. Seino, F. Bechstedt, S. Wippermann, W. G. Schmidt, A. Calzolari, and M. Buongiorno Nardelli, Phys. Rev. Lett. **98**, 026105 (2007).
[46] S. Wippermann and W. G. Schmidt, Surf. Sci. **603**, 247 (2009).
[47] P. H. Hahn, W. G. Schmidt, and F. Bechstedt, Phys. Rev. Lett. **88**, 016402 (2001).